Activity-dependent regulation of voltage-gated Na^+ channel expression in Mat-LyLu rat prostate cancer cell line

William J. Brackenbury and Mustafa B. A. Djamgoz

Neuroscience Solutions to Cancer Research Group, Division of Cell and Molecular Biology, Sir Alexander Fleming Building, Imperial College London, South Kensington Campus, London SW7 2AZ, UK

We have shown previously that voltage-gated Na^+ channels (VGSCs) are up-regulated in human metastatic disease (prostate, breast and small-cell lung cancers), and that VGSC activity potentiates metastatic cell behaviours. However, the mechanism(s) regulating functional VGSC expression in cancer cells remains unknown. We investigated the possibility of activity-dependent (auto)regulation of VGSC functional expression in the strongly metastatic Mat-LyLu model of rat prostate cancer. Pretreatment with tetrodotoxin (TTX) for 24–72 h subsequently suppressed peak VGSC current density without affecting voltage dependence. The hypothesis was tested that the VGSC auto-regulation occurred via VGSC-mediated Na^+ influx and subsequent activation of protein kinase A (PKA). Indeed, TTX pretreatment reduced the level of phosphorylated PKA, and the PKA inhibitor KT5720 decreased, whilst the adenylate cyclase activator forskolin and the Na^+ ionophore monensin both increased the peak VGSC current density. TTX reduced the mRNA level of Nav1.7, predominant in these cells, and VGSC protein expression at the plasma membrane, although the total VGSC protein level remained unchanged. TTX pretreatment eliminated the VGSC-dependent component of the cells' migration in Transwell assays. We concluded that the VGSC activity in Mat-LyLu rat prostate cancer cells was up-regulated in steady-state via a positive feedback mechanism involving PKA, and this enhanced the cells' migratory potential.

(Resubmitted 3 February 2005; accepted after revision 15 March 2006; first published online 16 March 2006)
Corresponding author M. B. A. Djamgoz: *Neuroscience Solutions to Cancer* Research Group, Division of Cell and Molecular Biology, Sir Alexander Fleming Building, Imperial College London, South Kensington Campus, London SW7 2AZ, UK. Email: m.djamgoz@imperial.ac.uk

Activity-dependent regulation of plasma membrane receptors and ion channels is well known to occur and is particularly important for development and maintenance of neural plasticity (Moody & Bosma, 2005). As regards voltage-gated Na^+ channels (VGSCs), regulation appears complex.

Activity-dependent regulation of VGSCs by negative feedback has been well documented. In fetal rat brain neurones, chronic treatment with VGSC 'opener' drugs including α-scorpion toxin (α-ScTX) down-regulated the α-subunit mRNA level, reduced VGSC expression at the cell surface, and induced protein internalization (Dargent & Couraud, 1990; Dargent *et al.* 1994; Lara *et al.* 1996; Paillart *et al.* 1996). Similarly, in developing mouse dorsal root ganglion (DRG) neurones, patterned stimulation significantly reduced Nav1.8 and Nav1.9 mRNA (Klein *et al.* 2003). This activity-dependent VGSC down-regulation was Na^+ dependent and could be mimicked by application of the Na^+ ionophores monensin and amphotericin B, and could be inhibited with the highly specific VGSC blocker tetrodotoxin (TTX) (Dargent & Couraud, 1990). Similarly, in bovine adrenal chromaffin cells, pharmacological blockade of electrical activity with the local anaesthetic bupivacaine potentiated VGSC translation and externalization (Shiraishi *et al.* 2003), and in developing rat skeletal myocytes, TTX or bupivacaine increased VGSC mRNA and cell surface protein expression (Sherman & Catterall, 1984; Offord & Catterall, 1989). There is also evidence for altered VGSC expression/activity by negative feedback in response to nerve injury (Waxman *et al.* 1994; Dib-Hajj *et al.* 1996; Black *et al.* 1999; Waxman, 2001).

In contrast, regulation of VGSCs by positive feedback appears to be much less common, and although functional VGSCs are expressed in a variety of cancer cells, it is not known if activity-dependent regulation, which could be important for disease progression, occurs. VGSC-expressing cancer cells include those of rat prostate (Grimes *et al.* 1995), human prostate (Laniado *et al.* 1997), human breast (Fraser *et al.* 2005), lymphoma (Fraser *et al.* 2004), small-cell lung cancer (Blandino *et al.* 1995; Onganer & Djamgoz, 2005) and melanoma (Allen *et al.*

 DOI: 10.1113/jphysiol.2006.106906

1997). VGSC up-regulation has similarly been found in human prostate cancer (PCa) and breast cancer *in vivo* (Abdul & Hoosein, 2002; Diss *et al.* 2005; Fraser *et al.* 2005). In the strongly metastatic rat (Mat-LyLu) and human (PC-3) PCa cell lines, the predominant VGSC isoform, Nav1.7, is up-regulated over 1000-fold at mRNA level, compared to the weakly metastatic counterpart cell lines, isogenic in the case of rat PCa (Diss *et al.* 2001).

In the present study, we investigated the possible activity-dependent regulation of VGSC/Nav1.7 expression in the rat Mat-LyLu model of PCa by testing the effect of chronic exposure to TTX on subsequent VGSC activity. Results indicated that basal VGSC activity was maintained in these cells by a *positive* feedback mechanism, with protein kinase A (PKA) as a key signalling intermediary. Preliminary findings from this study have been published previously (Brackenbury & Djamgoz, 2003, 2004, 2005).

Methods

Cell culture and pharmacological treatment

Mat-LyLu cells were cultured as previously described (Grimes & Djamgoz, 1998). Briefly, the cells were grown in Roswell Park Memorial Institute (RPMI) 1640 medium supplemented with 1% fetal bovine serum (FBS), 2 mM L-glutamine, 250 μg ml^{-1} amphotericin B and 250 nM dexamethasone. Cells were seeded into Falcon tissue culture dishes (Becton Dickinson) and incubated at 37°C, 5% CO_2 and 100% relative humidity. In some experiments, cells were incubated with the following pharmacological agents added into the growth medium 3 h post-seeding: tetrodotoxin (TTX; solvent: water; Alomone), KT5720 (solvent: DMSO; Calbiochem), forskolin (solvent: DMSO; Sigma) and monensin (solvent: ethanol; Sigma). Pharmacological agents were tested and determined to be non-toxic at their working concentrations using a trypan blue exclusion assay as previously described (Fraser *et al.* 2003).

Electrophysiology

Prior to recording, growth medium ± pharmacological agents was washed out by perfusing cells with external bath solution (144 mM NaCl, 5.4 mM KCl, 1 mM $MgCl_2$, 2.5 mM $CaCl_2$ 5.6 mM D-glucose and 5 mM Hepes, adjusted to pH 7.2 with 1 mM NaOH) for ∼15 min. Equimolar choline chloride was used as the substitute for NaCl in Na^+-free experiments. For 'short-term' PKA inhibition experiments, KT5720 (500 nM), which has been used previously in studies on a variety of cells, including cancer (Ungefroren *et al.* 1997; Yang *et al.* 2003; Yoshida *et al.* 2005), was added to the external bath solution 5 min prior to recording, which continued for < 20 min. Patch pipettes were made as previously described (Ding & Djamgoz, 2004) and were filled with an internal patch solution containing 5 mM NaCl, 145 mM CsCl, 2 mM $MgCl_2$, 1 mM $CaCl_2$, 10 mM Hepes, 11 mM EGTA, adjusted to pH 7.4 with 1 M CsOH.

Whole-cell patch clamp recordings were performed on single cells as described in detail previously (Grimes & Djamgoz, 1998) using Axopatch 1D patch clamp amplifier (Axon Instruments) compensating for series resistance by ∼80%. Currents were digitized using a Digidata 1200 interface (Axon Instruments), low-pass filtered at 5 kHz, sampled at 50 kHz, and analysed using pCLAMP 6 software (Axon Instruments). Linear components of leak were subtracted using the leak subtraction facility on the amplifier and/or using the pCLAMP software. Two voltage-clamp protocols were used (holding potential = −100 mV):

(1) Basic current–voltage (I–V) protocol: Cells were depolarized to test potentials within the range −70 to +70 mV in 5 mV steps. The test pulse duration was 60 ms; the interpulse duration was 2 s.

(2) Steady-state inactivation protocol: Prepulses in the range −130 to −10 mV were applied in 10 mV steps for durations of 1 s. A test pulse of −10 mV was immediately applied for 80 ms; the interpulse duration was 2 s.

Recordings were obtained from a minimum of 18 cells per condition, from at least three repeat treatments. Data from individual dishes were combined to provide an overall mean and standard error of the mean (S.E.M.). Conductance–voltage relationships and curve fitting were performed as previously described (Ding & Djamgoz, 2004).

Real-time PCR

Extraction of total RNA, synthesis of cDNA and real-time PCR were performed as previously described (Mycielska *et al.* 2005), with some modifications. Cytochrome b_5 reductase (Cytb5R) was measured as a control/reference gene to normalize the respective measured Nav1.7 expression. Cytb5R has been shown previously to remain unchanged in rat PCa (Diss *et al.* 2001). The Nav1.7 primers were: 5′-TTCATGACCTTGAGCAACCC-3′ and 5′-TCTCTTCGAGTTCCTTCCTG-3′; annealing temperature, 60°C; and the Cytb5R primers were: 5′-ACACGCATCCCAAGTTTCCA-3′ and 5′-CATCTCCTCATTCACGAAGC-3′; annealing temperature, 60°C (Diss *et al.* 2001). The threshold amplification cycles (C_T) were determined using the Opticon Monitor 2 software (MJ Research) and then analysed by the $2^{-\Delta\Delta C_T}$ method (Livak & Schmittgen, 2001). The relative expression of Nav1.7 (mRNA) was compared with untreated control cells, for at least three separate treatments.

Western blotting

Cell lysates were prepared in modified radioimmunoprecipitation (RIPA) buffer (Sigma) plus 1 mM PMSF, 1 μg ml^{-1} aprotinin, 1 μg ml^{-1} leupeptin,

1 μg ml^{-1} pepstatin and 1 mM NaF. Protein yield was determined using a Bradford dye binding assay (Bio-Rad), according to the manufacturer's guidelines. Equivalent amounts of protein from different lysate samples (60 μg/well) were resolved against a wide range (C3437) colour marker (Sigma) by sodium dodecyl sulphate polyacrylamide gel electrophoresis (SDS-PAGE), as previously described (Laniado *et al.* 1997). Briefly, lysates were prepared in sample buffer containing 35% glycerol, 10% SDS, 250 mM DTT, with bromophenol blue, according to the manufacturer's guidelines for specific antibodies (Upstate, Sigma). Electrophoresis was performed using 6% acrylamide gels in a buffer containing 25 mM Tris, 192 mM glycine, and 0.1% SDS at 160 V for 6 h. Protein was transferred to nitrocellulose membrane at 4°C in a buffer containing 25 mM Tris and 192 mM glycine at 25 V for 16 h. Nitrocellulose membranes were blocked for 1 h in 5% (w/v) non-fat dried milk/phosphate-buffered saline (PBS), followed by 30 min in 2% (w/v) bovine serum albumen (BSA)/PBS. Three primary antibodies were used, diluted in 2% (w/v) BSA/PBS, to final concentrations, as follows:

(1) pan-VGSC antibody (1 μg ml^{-1}; Upstate),

(2) anti-phosphorylated PKA antibody (1 μ1 ml^{-1}; Upstate), and

(3) anti-actinin antibody (1 μl ml^{-1}; Sigma).

The secondary antibodies for (1) and (2) were peroxidase-conjugated swine anti-rabbit, and goat anti-mouse for (3) (Dako). Blots were developed using the ECL chemiluminescence system (Amersham) and visualized by exposure to Super RX100NF film (Fujifilm). Densitometric analysis was performed using Image-Pro Plus software (Media Cybernetics). For all three antibodies, linearity of signal intensity with respect to protein concentration within the range 20 μg ml^{-1} to 80 μg ml^{-1} was ensured using serial dilutions of control protein lysate. Signal density was normalized to anti-actinin antibody as a loading control/reference, for at least five separate treatments.

Immunocytochemistry and confocal microscopy

Cells (2×10^4) were seeded onto poly L-lysine coated glass coverslips for 48 h and then fixed in 4% (w/v) paraformaldehyde/PBS. Cells were labelled first with 0.2 mg ml^{-1} fluorescein isothiocyanate (FITC)-conjugated concanavalin A (Sigma) in 5% BSA/PBS, for 30 min as a plasma membrane marker, then permeabilized in 0.1% (w/v) saponin/PBS for 5 min. Non-specific binding sites were blocked for 1 h with 5% BSA/PBS and then cells were incubated with the primary antibody (pan-VGSC, 1 : 100; Upstate) for 1 h, followed by the Alexa567-conjugated goat anti-rabbit secondary antibody (1 : 100; Dako) for 1 h. Cells were then mounted in Vectashield mounting medium (Vector Laboratories).

Cells were examined on a Leica DM IRBE microscope with ×100 objective and a Leica confocal laser scanner (Leica TCS-NT with Ar/Kr laser). FITC and/or Alexa567 were excited with the 488 nm and 568 nm laser lines, respectively. The images (512 pixels × 512 pixels) were obtained simultaneously from two channels using a confocal pinhole of 226.98 μm (Airy 1).

Digital analysis

Densitometric analysis was performed using the LCS Lite software (Leica), as follows.:

(1) Cell surface protein level was initially quantified using the 'freeform line profile' function drawn around the cell surface, determined by concanavalin A staining. Measurements were taken from 20 to 30 cells (randomly chosen) per condition, for three repeat treatments.

(2) The subcellular distribution of VGSC protein was determined using the 'straight line profile' function drawn across the cytoplasm avoiding the nucleus, extending the original methodologies of Okuse *et al.* (2002) and Shah *et al.* (2004). Signal intensity in plasma membrane region, set to cover 1.5 μm inward from the edge of concanavalin A staining, was compared with cytoplasmic signal intensity within the central 30% of the line profile. Measurements were taken from ≥ 6 cells (randomly chosen) per condition, for three repeat treatments.

Migration assay

Cells (1.5×10^5 cells ml^{-1}) pretreated with/without TTX (1 μM) for 48 h were plated onto 12 μm Transwell pore filters in a 12-well plate, according to the manufacturer's instructions (Corning), in a 0.1–1% FBS chemotactic gradient (Fraser *et al.* 2005), and incubated with/without TTX (1 μM) for 7 h. The number of cells migrating over 7 h was determined using the MTT assay (Grimes *et al.* 1995). Results were compiled as the mean of four repeats of drug *versus* control readings for duplicate platings.

Data analysis

All quantitative data are presented as means ± standard error of the mean (S.E.M.), unless stated otherwise. Statistical significance was determined with Student's *t* test, or ANOVA followed by Newman-Keuls *post hoc* analysis, as specified in Results. Comparison of linear regression slopes was performed using the *t* test method for regression slope, as follows:

$$t = (\text{slope } 1 - \text{slope } 2)/\sqrt{[(\text{S.E.M. slope } 1)^2 + (\text{S.E.M. slope } 2)^2]}.$$

Real-time PCR data were analysed using the $2^{-\Delta\Delta C_T}$ method (Livak & Schmittgen, 2001). Results were considered significant at $P < 0.05$ (*).

Results

Pre-incubation with TTX suppressed VGSC functional activity

Mat-LyLu cells were preincubated for 24–72 h with TTX (1 μM) in order to chronically block all VGSC activity (Grimes & Djamgoz, 1998). TTX was removed prior to recording by perfusion with external bath medium for 15 min. Superfusion with a Na^+-free external medium during recording completely abolished inward currents in control cells and cells that had been preincubated for 48 h with TTX, consistent with all the recorded inward currents being due to VGSC activity. In order to confirm that TTX had effectively been removed prior to recording, peak VGSC current densities for control or TTX-pretreated cells were monitored for any change during the 70 min recording period (Fig. 1*B*). The linear regression slopes for control and TTX pretreated cells were not significantly different from horizontal ($P = 0.99$ for both), and were not significantly different from each other ($P = 0.99$), consistent with TTX having been removed prior to the recording. Indeed, short-term TTX perfusion experiments showed that TTX reversed within seconds of washout (data not shown).

Pretreatment with TTX for 24 h significantly reduced peak VGSC current density by 56% from 22.1 ± 2.4 to 9.7 ± 1.7 pA pF^{-1} ($P < 0.001$; *t* test; $n > 20$ for each) and the effect was maintained for 72 h (Fig. 1*A* and *C*). The TTX pretreatment had no effect on activation voltage, voltage for current peak, voltage dependence of activation or steady-state inactivation (Fig. 1*D* and *E*). There was a window current between −60 mV and −20 mV and this was also not affected by the TTX pretreatment (Fig. 1*D* inset). Pre-incubation with a lower (20 nM) concentration of TTX, close to the IC_{50} (Grimes & Djamgoz, 1998) for 72 h had no effect on peak VGSC current density recorded subsequently. When cells were preincubated in TTX (1 μM) for 48 h and then allowed to recover for a further 24 h in normal culture medium prior to recording, the inhibition of inward currents was found to be fully reversible.

From these data and the available evidence, we proposed the following basic hypothesis for activity-dependent steady-state regulation of VGSCs in Mat-LyLu cells: VGSC → Na^+ influx → PKA activation (Cooper *et al.* 1998; Murakami *et al.* 1998) → increased functional VGSC availability (Yuhi *et al.* 1996; Zhou *et al.* 2000; Wada *et al.* 2004). This hypothesis/scheme was tested systematically in a variety of ways, focusing upon the peak VGSC current density, as follows.

PKA modulated VGSC peak current amplitude

Short-term (5–20 min) superfusion of a PKA inhibitor (KT5720; 500 nM) resulted in an increase in peak VGSC current density from 30.1 ± 3.5 to 48.4 ± 5.8 pA pF^{-1} ($P < 0.05$; *t* test; $n = 18$ for each). This is in agreement with previous findings (Li *et al.* 1992; Cantrell *et al.* 1997; Smith & Goldin 1997; Vijayaragavan *et al.* 2004) and confirmed the effectiveness of the KT5720 treatment.

Long-term (48 h) preincubation with KT5720 (500 nM), as with TTX, suppressed peak VGSC current density by 56% from 17.6 ± 2.0 to 7.7 ± 1.7 pA pF^{-1} ($P < 0.01$; ANOVA with Newman-Keuls; $n = 20$ for each). This effect was dose dependent (Fig. 2*A*). Pre-incubation with the adenylate cyclase (AC) activator forskolin (50 μM) for 48 h had the opposite effect, increasing peak VGSC current density by 96% from 23.7 ± 2.6 to 46.5 ± 5.8 pA pF^{-1} ($P < 0.01$; *t* test; $n = 18$ for each; Fig. 2*B*).

We concluded that, in the long term, PKA activity increased VGSC current density, consistent with the proposed model.

Pre-incubation with monensin increased VGSC functional activity

The Na^+ ionophore monensin was used in order to directly raise the intracellular Na^+ level (Harootunian *et al.* 1989). Pre-incubation with monensin (10 nM) for 48 h increased peak VGSC current density by 55% from 19.8 ± 2.4 to 30.6 ± 3.9 pA pF^{-1} ($P < 0.05$; *t* test; $n = 24$ for each; Fig. 3*A*). Co-application of TTX with monensin or forskolin each counter-acted the effect of TTX alone on peak VGSC current density (Fig. 3*B*). Thus, the peak VGSC current density for TTX + monensin, or TTX + forskolin was not significantly different from the control ($P = 0.18$ and 0.52, respectively; ANOVA with Newman-Keuls; $n = 23$ for each; Fig. 3*B*). Conversely, when coapplied with KT5720, monensin did not significantly increase the peak current density, compared with KT5720 alone ($P = 0.45$; ANOVA with Newman-Keuls; $n = 20$ for each; Fig. 3*C*).

Western blot on total protein extracts with a phosphorylated PKA antibody was used to test the effect of TTX treatment on the level of phosphorylated PKA. A control confirmed that treatment with KT5720 (500 nM) for 48 h almost completely eliminated PKA phosphorylation (Fig. 3*D*, lane 3). Treatment with TTX (1 μM) for 48 h reduced the level of phosphorylated PKA by 35% ($P < 0.01$; paired *t* test; $n = 8$) (Fig. 3*D* lane 1 *versus* lane 2; Fig. 3*E*).

These data further supported the proposed hypothesis that activation of PKA by VGSC activity/Na^+ influx resulted in up-regulation of VGSC activity. We next tested at what level (mRNA and/or protein) the auto-regulation of VGSCs occurred, focusing on Nav1.7, the predominant form of VGSC expressed in PCa cells (Diss *et al.* 2001).

TTX and KT5720 both reduced Nav1.7 mRNA level

Mat-LyLu cells were incubated with TTX for 48 h, after which the mRNA level of Nav1.7 was assessed

by real-time polymerase chain reaction (rt-PCR). Pretreatment with TTX (1 μM) significantly reduced the Nav1.7 mRNA level by 52% ($P < 0.05$; ANOVA with Newman-Keuls; $n = 4$), whereas 20 nM TTX had no effect ($P = 0.69$; ANOVA with Newman-Keuls; $n = 3$; Fig. 4*A* and *B*). Similarly, pretreatment with KT5720 (500 nM) significantly reduced the Nav1.7 mRNA level by 45% ($P < 0.05$; ANOVA with Newman-Keuls; $n = 4$). Co-application of KT5720 and TTX did not reduce Nav1.7 mRNA further than either TTX or KT5720 alone ($P = 0.98$; ANOVA with Newman-Keuls; $n = 3$; Fig. 4*A* and *C*).

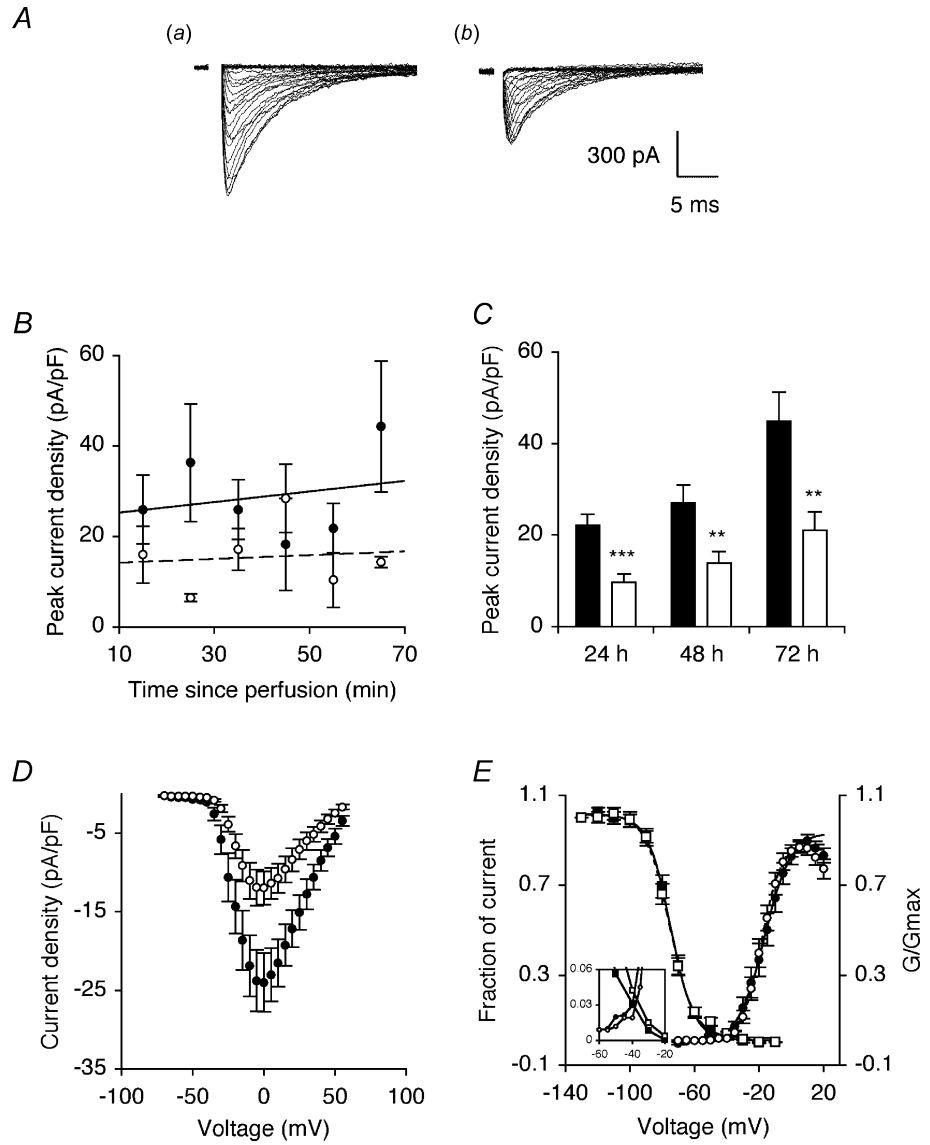

Figure 1. TTX pretreatment reduced peak VGSC current density
A, typical whole-cell VGSC currents elicited by 60 ms depolarizing voltage pulses between −70 mV and +70 mV applied from a holding potential of −100 mV: *a*, control cell; *b*, cell pretreated with 1 μM TTX for 48 h. *B*, peak VGSC current density of control cells and cells pretreated with 1 μM TTX for 48 h, recorded in sequential order, post perfusion of external bath medium. Control (continuous line; equation: $y = 0.12x + 21.2$) and TTX data (dotted line; equation: $y = 0.04x + 13.8$) are fitted with linear regressions. *C*, quantitative comparison of peak current densities recorded in control cells (filled bars), and cells pretreated with 1 μM TTX for 24–72 h (open bars). *D*, mean current–voltage relationships for control cells (●), and cells pretreated with 1 μM TTX for 48 h (○). *E*, mean availability–voltage (squares) and relative conductance (G/G_{max})–voltage relationships (circles) for control cells (filled symbols) and cells pretreated with 1 μM TTX for 48 h (open symbols). Control (continuous lines) and TTX data (dotted lines) are fitted with Boltzmann functions. The inset magnifies a window in which current is activated and not fully inactivated. Data are presented as means ± S.E.M. ($n = 18$ for all, except *B*: $n = 4$). Significance: $^{**}P < 0.01$, $^{***}P < 0.001$.

We concluded that the VGSC auto-regulation mechanism involved regulation of Nav1.7 mRNA level, and that PKA was involved in this process.

TTX decreased plasma membrane VGSC protein level and suppressed VGSC-dependent migration

Western blot with a pan-specific VGSC α-subunit antibody revealed that treatment with TTX (1 μM) for 48 h did not reduce the total VGSC protein level (Fig. 5*A* and *B*). Confocal immunocytochemistry with the pan-VGSC antibody was used to assess the effect of TTX on the subcellular distribution of VGSC protein. As shown in Fig. 5*C*, cross-sections were taken across the cytoplasm of immunofluorescent cells avoiding the nucleus, as previously described (Okuse *et al.* 2002; Shah *et al.* 2004). Cells were labelled with the plasma membrane marker concanavalin A in order to identify the cell edge in cross-sections. In control cells, the cross-sections typically showed peaks of high immunofluorescence at the edge, in the plasma membrane region, whereas the TTX pretreatment shifted the VGSC immunoreactivity inward, away from the cell periphery (Fig. 5*Da versus b*).

The VGSC immunoreactivity along cell cross-sections was quantified in two regions: (1) 'plasma membrane', in a 1.5 μm section inward from the edge of concanavalin A staining (Okuse *et al.* 2002); and (2) 'internal', in the middle 30% of the cross-section. TTX reduced the level of VGSC protein in the plasma membrane region, from $6.1 \pm 0.9\%$ to $1.9 \pm 0.3\%$ of total immunofluorescence across the cross-section ($P < 0.001$; *t* test; $n = 20$ for each; Fig. 5*E*, left-hand bars). There was an opposite effect of TTX on the internal region: TTX increased immunofluorescence, from $37.0 \pm 1.7\%$, to $45.6 \pm 1.8\%$ ($P < 0.01$; *t* test; $n = 20$ for each; Fig. 5*E*, right-hand bars). In a second method, the plasma membrane VGSC level was quantified along freeform line profiles drawn around the edges of cells determined by the concanavalin A staining. TTX again caused a 32% reduction in VGSC immunoreactivity detected along the plasma membrane; this effect was highly significant ($P < 0.001$; *t* test; $n = 90$). These data were consistent with TTX inhibiting the trafficking of VGSC protein to the plasma membrane, without affecting the total protein level, so that protein accumulated in intracellular compartment(s).

Migration through 12 μm-pore Transwell filters was used as a measure of metastatic potential. Pretreatment with TTX (1 μM) for 48 h significantly reduced the number of cells migrating through the filter by 61% from $6.3 \pm 1.5 \times 10^3$ cells to $2.5 \pm 0.6 \times 10^3$ cells ($P < 0.05$; ANOVA with Newman-Keuls; $n = 4$; Fig. 6, bars 1 *versus* 2). When TTX was applied while the (non-pretreated) cells were migrating, their migration was reduced by 58% to $2.6 \pm 0.8 \times 10^3$ cells ($P < 0.05$; ANOVA with Newman-Keuls; $n = 4$; Fig. 6, bar 1 *versus* 3). Importantly, following the 48 h TTX pretreatment, TTX applied also during the assay had no further effect on migration ($P = 0.99$; ANOVA with Newman-Keuls; $n = 4$; Fig. 6, bar 3 *versus* 4). Thus, the VGSC-sensitive component of migration was suppressed completely by the long-term (48 h) pretreatment with TTX, in agreement with the reduced VGSC expression in the plasma membrane (Fig. 5*E*).

Discussion

The overall conclusion of this study is that functional VGSC expression in the strongly metastatic Mat-LyLu rat PCa cell line is under activity-dependent control by positive feedback. Thus, basal activity with feedback would maintain an elevated level of VGSC expression in steady state. As regards the mechanism underlying the effect, the following specific conclusions for long-term (24–72 h) regulation of VGSC current density were reached: (1) VGSC blockage reduced PKA activity. (2) Pharmacological inhibition of PKA decreased VGSC current density. (3) Activation of AC/PKA increased VGSC current density. (4) Elevation of $[Na^+]_i$ increased current density. (5) VGSC blockage reduced Nav1.7 mRNA level and VGSC protein at the plasma membrane, without affecting the total VGSC protein level. (6) Long-term VGSC blockage completely

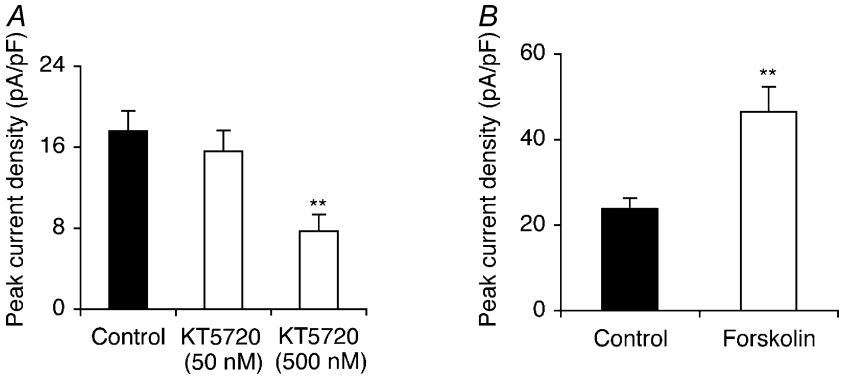

Figure 2. KT5720 pretreatment reduced and forskolin pretreatment increased peak VGSC current density
A, quantitative comparison of peak current densities recorded in control cells and cells pretreated with KT5720 (50 or 500 nM) for 48 h. *B*, quantitative comparison of peak current densities recorded in control cells and cells pretreated with 50 μM forskolin for 48 h. Data are presented as means ± S.E.M. ($n = 20$). Significance: $^{**}P < 0.01$, $^{***}P < 0.001$.

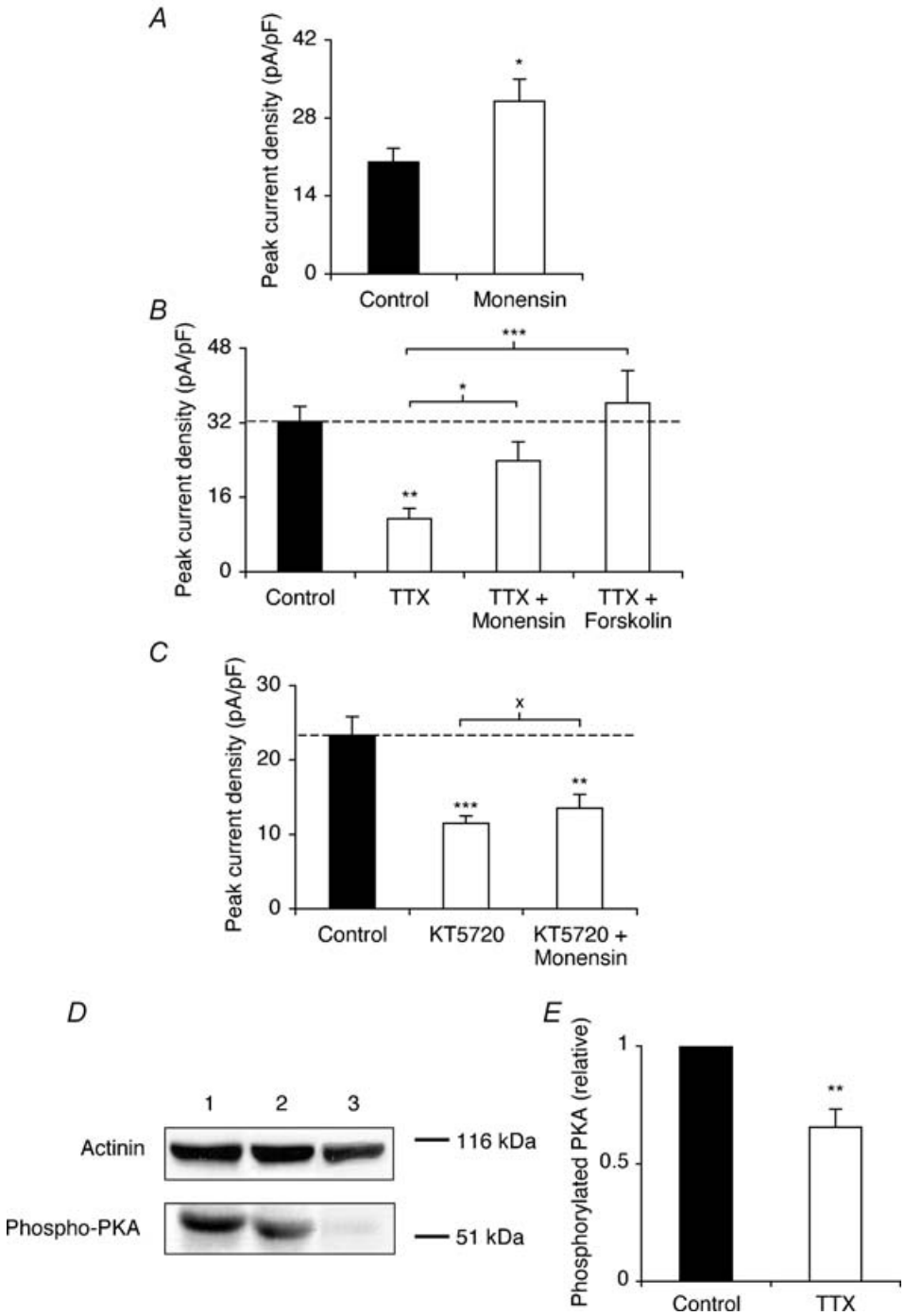

Figure 3. Monensin increased VGSC activity, and monensin and forskolin reversed the inhibiting effect of TTX pretreatment on VGSC activity

A, quantitative comparison of peak current densities recorded in control cells and cells pretreated with 10 nM monensin for 48 h. *B*, peak current densities recorded after pretreatment for 48 h in control conditions, or with TTX (1 μM) with or without monensin (10 nM) or forskolin (50 μM). *C*, peak current densities recorded after pretreatment for 48 h in control conditions, or with KT5720 (500 nM) with or without monensin (10 nM). *D*, Western blot with 60 μg of total protein per lane from control cells, cells treated with TTX (1 μM) for 48 h, and cells treated with KT5720 (500 nM) for 48 h, using a phosphorylated PKA antibody, and an actinin antibody for loading control. *E*, relative phosphorylated PKA level in control cells and cells treated with TTX (1 μM) for 48 h. Data are presented as means and S.E.M. ($n = 20$ for all, except *E*: n = 8). Significance: $^{X}P > 0.05$, $^{*}P < 0.05$, $^{**}P < 0.01$, $^{***}P < 0.001$.

suppressed the VGSC-dependent component of migration *in vitro*.

Effects of TTX and monensin on VGSC expression/activity

Blocking VGSC activity with TTX, thus suppressing the voltage-dependent influx of Na^+ into the cell, resulted in reduction of VGSC activity. Importantly, voltage dependence (Fig. 1*D* and *E*) and kinetics (data not shown) did not change as a result of the TTX treatment, suggesting that the change in current amplitude did not involve a biochemical modification, such as phosphorylation. In order to determine whether $[Na^+]_i$ was involved, monensin, an electroneutral Na^+/H^+ carboxylic acid ionophore typically used for Na^+ loading in cellular studies was used (e.g. Dargent & Couraud, 1990; Buchanan *et al.* 2002). After 48 h pretreatment, monensin increased VGSC current density, opposite to the effect of TTX. Furthermore, coapplication of monensin with TTX almost entirely reversed the inhibitory effect of the TTX pretreatment on peak VGSC current density.

We concluded that elevation of $[Na^+]_i$ via VGSC activity would provide a signal for positive feedback autoregulation of VGSC activity and this cycle could be suppressed using TTX. The feedback effect was apparent only after complete VGSC blockage implying that it served an 'all-or-none' function. We should also note that Na^+ influx through VGSCs is likely to be localized within specific microdomains, whereas monensin activity would result in a global elevation of $[Na^+]_i$, which may induce additional changes in intracellular Ca^{2+} and/or pH (Wakabayashi *et al.* 2003).

VGSC regulation at mRNA and protein levels

Long-term treatment with TTX or the PKA inhibitor KT5720 reduced the Nav1.7 mRNA level. Their effects were not additive, consistent with their influencing components of the same signalling pathway. Surprisingly, the mRNA-level reduction was not reflected at the total VGSC protein level. However, increasing evidence suggests that regulation of mRNA and protein levels can be separate and independent (e.g. Orphanides & Reinberg,

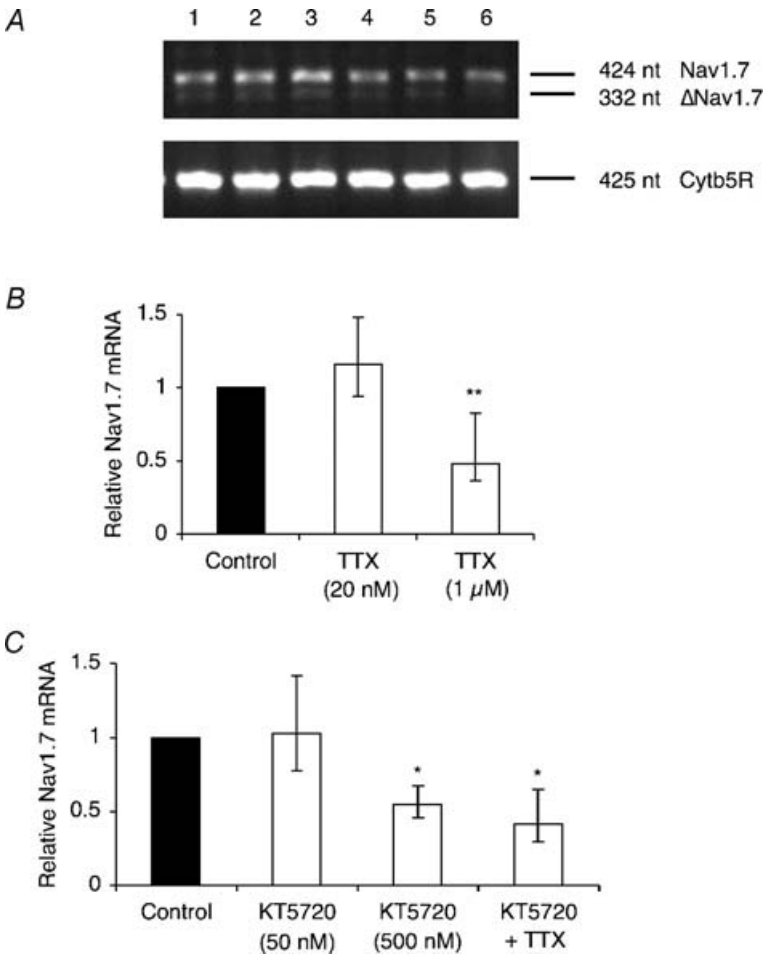

Figure 4. TTX and KT5720 reduced the Nav1.7 mRNA level
A, typical gel images of PCR products for Nav1.7 and cytochrome b_5 reductase (Cytb5R). Lanes: 1, control; 2, pretreated for 48 h with TTX (20 nM); 3, TTX (1 μM); 4, KT5720 (50 nM); 5, KT5720 (500 nM); 6, KT5720 (500 nM) and TTX (1 μM). Δ denotes exon-skipped Nav1.7. *B*, relative Nav1.7 mRNA levels in control cells and cells treated for 48 h with TTX (20 nM or 1 μM). *C*, relative Nav1.7 mRNA levels in control cells and cells treated for 48 h with KT5720 (50 nM or 500 nM), or with KT5720 (500 nM) + TTX (1 μM). KT5720 (50 nM) bar is included here for completeness (complementing the data in Fig. 2*A*), but was not incorporated into the statistical analysis. Nav1.7 expression was normalized to Cytb5R by the $2^{-\Delta\Delta C_T}$ method. Errors are propagated through the $2^{-\Delta\Delta C_T}$ analysis ($n = 3$). Significance: $^*P < 0.05$, $^{**}P < 0.01$.

2002). Discrepancies between mRNA and protein levels have also been reported in a variety of disease states, including cancer (Sola *et al.* 1999; Schedel *et al.* 2004; Gu *et al.* 2006). Instead, post-transcriptional mechanisms including mRNA localization/docking, and/or protein translation/trafficking may play an important role (Tiedge *et al.* 1999; Ben Fredj *et al.* 2004; St Johnston, 2005).

The TTX treatment altered the subcellular distribution of VGSC protein detected by confocal immunocytochemistry, such that there was a reduction of protein

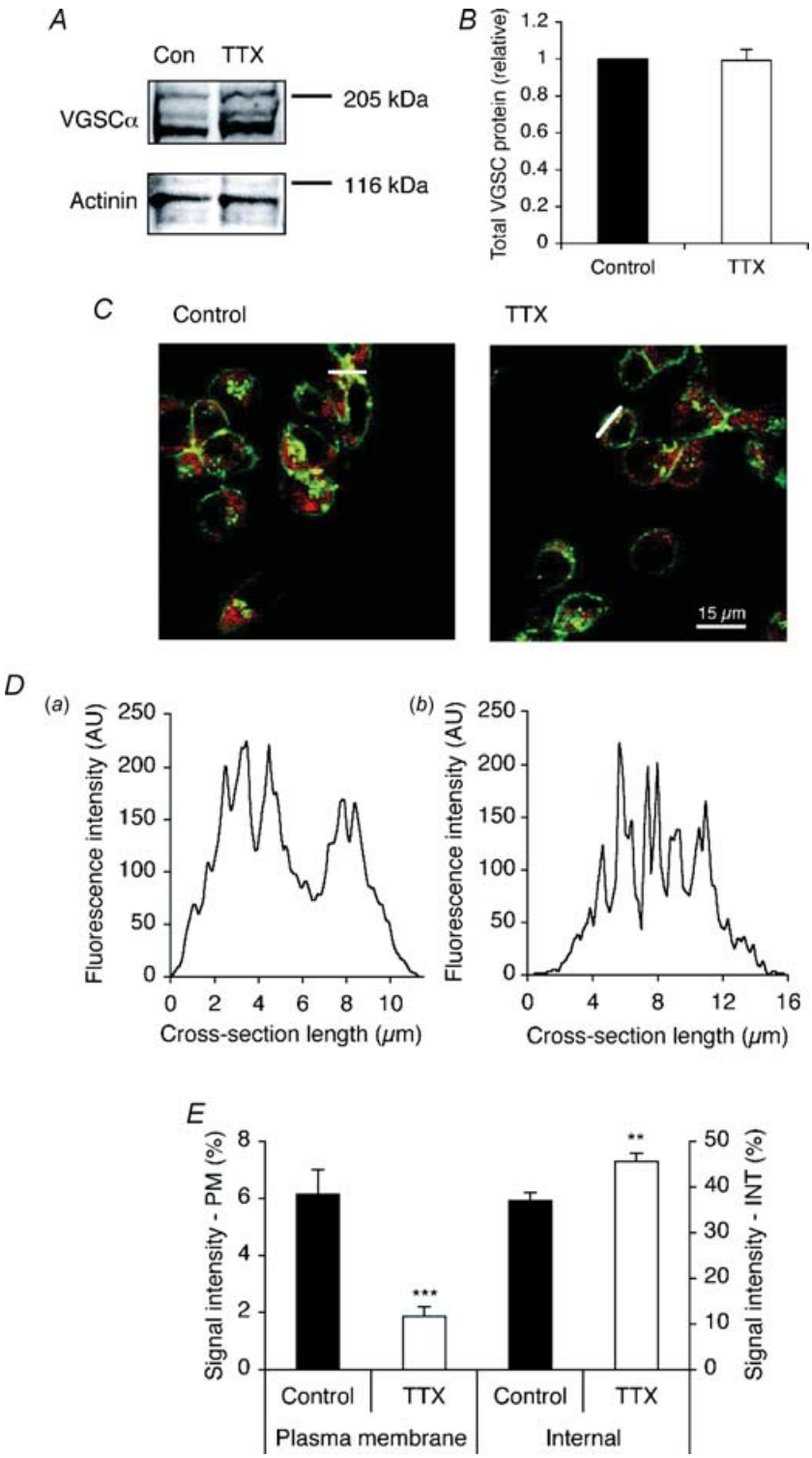

Figure 5. TTX did not affect the total VGSC protein level, but reduced the level of VGSC protein at the cell surface
A, Western blot with 60 μg of total protein per lane from cells treated with or without TTX (1 μM) for 48 h, using a pan-VGSC antibody, and an actinin antibody as a control for loading. *B*, relative total VGSC protein level in control cells and cells treated with TTX (1 μM) for 48 h. The VGSC α-subunit protein level was normalized to the actinin control. *C*, typical confocal images of control cells and cells treated with TTX for 48 h, double-immunolabelled with pan- VGSC antibody (red) and concanavalin A plasma membrane marker (green). White bars, cross-sections used for *D*. *D*, pan-VGSC immunofluorescence along cross-sections from a typical control cell (*a*), and cell treated with TTX (1 μM) for 48 h (*b*). AU, arbitrary unit. *E*, VGSC α-subunit protein distribution along subcellular cross-sections (%). Left-hand bars, 1.5 μm sections measured inward from edge of concanavalin A staining; right-hand bars, middle 30% of cross-section. PM, plasma membrane; INT, internal. Data are presented as means and S.E.M. (*B*, $n = 5$; *E*, $n = 20$). Significance: $^{**}P < 0.01$, $^{***}P < 0.001$.

at the plasma membrane, with an associated increase of protein in subcellular region(s). This result was confirmed by the reduction in VGSC current density after 24 h pretreatment with TTX, close to the previously reported half-life of VGSC protein, 18–26 h (Waechter *et al.* 1983; Sherman *et al.* 1985). Taken together, the simplest explanation of these data is that TTX altered the recycling of VGSC proteins, resulting in net inhibition of VGSC trafficking to the cell surface, such that the protein was retained in internal membranes.

Involvement of PKA in VGSC autoregulation

It has been reported that Na^+ could directly increase PKA activity, independent of Ca^{2+}, by activating AC (Cooper *et al.* 1998; Murakami *et al.* 1998). Consistent with this, treatment of Mat-LyLu cells with TTX for 48 h significantly reduced the level of phosphorylated PKA, suggesting that VGSC-dependent elevation of $[Na^+]_i$ did indeed activate PKA. Furthermore, treatment for 48 h with the AC activator forskolin increased peak VGSC current density, whereas the PKA inhibitor KT5720 reduced peak VGSC current density, suggesting that PKA potentiated VGSC functional availability. Importantly, forskolin reversed the inhibiting effect of TTX, whereas KT5720 inhibited the potentiating effect of monensin, on peak VGSC current density. Together, these data provide compelling evidence that PKA was indeed a downstream signalling intermediate in the positive-feedback activity-dependent regulation of VGSC functional expression.

Acute application of KT5720 increased peak current density, consistent with the previously reported effect of PKA phosphorylation on Nav1.7 (Vijayaragavan *et al.* 2004). Long-term treatment with KT5720 caused complete loss of phosphorylated PKA, probably due to the potency, the broad profile (amongst possible PKA subtypes), and the concentration of the inhibitor used. This is consistent with the effectiveness of KT5720 in the range of cells tested and reported earlier (e.g. Ungefroren *et al.* 1997; Yang *et al.* 2003; Yoshida *et al.* 2005). Interestingly, TTX (which reduced phosphorylated PKA by 35%) and KT5720 (which almost completely blocked it), produced a similar reduction in the VGSC current density (∼50% of control levels). These imply that there could be multiple PKAs in the cells in terms of subtype(s) of enzyme, and/or spatial localization/microdomains (Smith *et al.* 2006).

There is evidence to suggest that PKA could be involved in both protein trafficking and transcriptional processes responsible for maintaining tonically active VGSCs at the plasma membrane. Accordingly, treatment of developing rat muscle cells with 8-Br-cAMP for 8 days increased the VGSC α-subunit mRNA level (Offord & Catterall, 1989). Similarly, chronic (>12 h) treatment with forskolin or dibutryl-cAMP has been shown to increase cell surface VGSC availability in bovine adrenal chromaffin and rat muscle cells (Sherman *et al.* 1985; Yuhi *et al.* 1996; Wada *et al.* 2004). Although the mechanism(s) involved are not yet clear, PKA activity has been shown to regulate budding of vesicles from the *trans*-Golgi network along the exocytic route to the cell surface (Muniz *et al.* 1996, 1997).

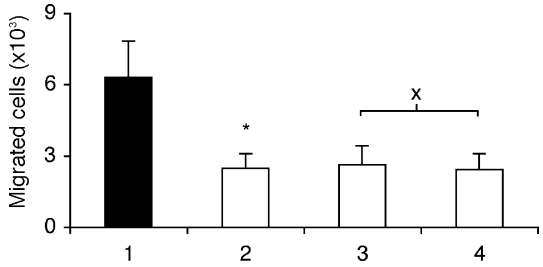

Figure 6. Pretreatment with TTX eliminated VGSC-dependent migration
The figure shows the number of cells migrating through a Transwell chamber over 7 h. Bar labels: 1, control pretreated cells; 2, cells pretreated with TTX (1 μM) for 48 h; 3, control pretreated cells migrated in presence of TTX (1 μM); 4, cells pretreated with TTX and then migrated in presence of TTX. Data are presented as means and S.E.M. Significance: $^{X}P > 0.05$; $^{*}P < 0.05$; $n = 4$.

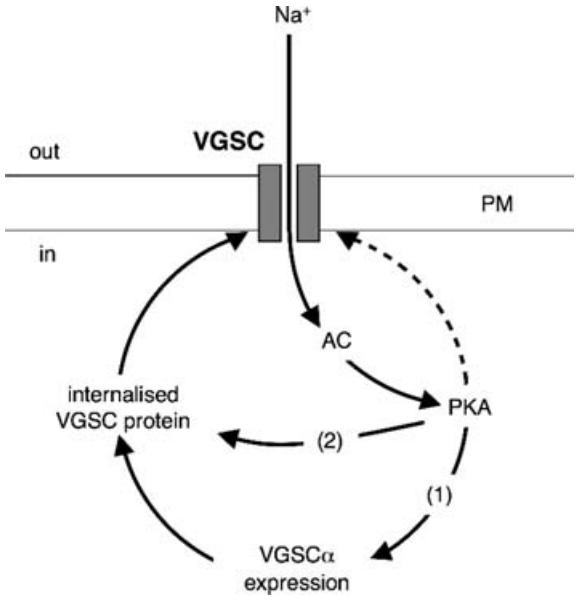

Figure 7. A basic model of activity-dependent, steady-state regulation of functional VGSC expression in Mat-LyLu cells by positive feedback (continuous lines)
Influx of Na^+ through VGSCs results in activation of AC and PKA. PKA can have multiple effects on VGSC expression in plasma membrane (PM): (1) potentiation of *de novo* VGSC synthesis via transcription; and (2) increased trafficking of VGSC protein to the plasma membrane. In addition, PKA can directly phosphorylate surface-expressed VGSCs (dashed line), although this may be independent of Na^+.

A model of activity-dependent regulation of VGSC functional expression by positive feedback

In the light of our findings, together with the published data, a model of activity-dependent regulation of VGSC functional expression by positive feedback in Mat-LyLu cells can be proposed (Fig. 7). Accordingly, local Na^+ influx through VGSCs causes activation of PKA, which in turn may stimulate VGSC transcription, and/or potentiate trafficking of VGSC protein to the plasma membrane.

It should be noted that other PKA-dependent mechanisms might also impinge on this regulatory pathway. Indeed, PKA may influence transcription of a large number of genes (Zhang *et al.* 2005). In addition, we cannot rule out the possible involvement of, and interaction with, other protein kinases, e.g. mitogen-activated protein kinase (Chang *et al.* 2006; Jin & Chang, 2006), Ca^{2+}/calmodulin (Herzog *et al.* 2003; Kim *et al.* 2004), and Src kinase (Hilborn *et al.* 1998). Nevertheless, the high consistency of the PKA data in our study would suggest that the basic model described is robust.

Pathophysiological implications

Treatment with TTX has been shown to suppress a variety of *in vitro* cell behaviours associated with the metastatic cascade, including morphological development and cellular process extension (Fraser *et al.* 1999), galvanotaxis (Djamgoz *et al.* 2001), lateral motility (Fraser *et al.* 2003), endocytic membrane activity (Mycielska *et al.* 2003) including vesicular patterning (Krasowska *et al.* 2004), adhesion (unpublished observations), gene expression (Mycielska *et al.* 2005) and invasion (Grimes *et al.* 1995; Laniado *et al.* 1997; Smith *et al.* 1998; Bennett *et al.* 2004). In fact, Bennett *et al.* (2004) concluded that functional VGSC expression was 'necessary and sufficient' for potentiation of prostate cancer cell invasiveness. Furthermore, VGSC blockers have been shown to inhibit PCa cell proliferation (Abdul & Hoosein, 2002; Anderson *et al.* 2003), and the VGSC-blocking anticonvulsants phenytoin and carbamazepine were found to directly inhibit secretion of prostate-specific antigen (PSA) and interleukin-6 by LNCaP and PC-3 PCa cell lines, respectively (Abdul & Hoosein, 2001). Taken together, these findings imply that VGSCs are tonically active in metastatic PCa cells, and have led to a new concept that PCa metastasis has some of the key features of cellular 'excitability'. Regulation of VGSC expression/activity by positive feedback would potentiate the multistage metastatic process (Fidler, 2003). Interestingly, this activity-dependent component operated in an all-or-none fashion, implying that it served as a switching mechanism. In fact, breaking the tonic positive feedback loop maintaining VGSC activity by suppressing VGSCs with long-term (48 h) TTX treatment completely eliminated the VGSC-dependent component of the cells' metastatic potential.

This is the first study demonstrating activity-dependent regulation of functional VGSC expression in a cancer cell line. Importantly, unlike the majority of previous reports in non-cancer cells (e.g. Dargent & Couraud, 1990), the feedback was positive, suggesting that VGSC activity-dependent regulation of VGSCs in PCa cells may operate differently to ensure a high level of VGSC expression and thus to maximize contribution to metastatic cell behaviour enhancement. This functional output has important clinical implications, whereby long-term VGSC blockage in PCa using non-cytotoxic drugs (Anderson *et al.* 2003), could result in direct short-term inhibition and long-term down-regulation. Thus, the VGSC would appear to have the hallmarks of an effective target for long-term control/suppression of metastatic PCa.

References

Abdul M & Hoosein N (2001). Inhibition by anticonvulsants of prostate-specific antigen and interleukin-6 secretion by human prostate cancer cells. *Anticancer Res* **21**, 2045–2048.

Abdul M & Hoosein N (2002). Voltage-gated sodium ion channels in prostate cancer: expression and activity. *Anticancer Res* **22**, 1727–1730.

Allen DH, Lepple-Wienhues A & Cahalan MD (1997). Ion channel phenotype of melanoma cell lines. *J Membr Biol* **155**, 27–34.

Anderson JD, Hansen TP, Lenkowski PW, Walls AM, Choudhury IM, Schenck HA, Friehling M, Holl GM, Patel MK, Sikes RA & Brown ML (2003). Voltage-gated sodium channel blockers as cytostatic inhibitors of the androgen-independent prostate cancer cell line PC-3. *Mol Cancer Ther* **2**, 1149–1154.

Ben Fredj N, Grange J, Sadoul R, Richard S, Goldberg Y & Boyer V (2004). Depolarization-induced translocation of the RNA-binding protein Sam68 to the dendrites of hippocampal neurons. *J Cell Sci* **117**, 1079–1090.

Bennett ES, Smith BA & Harper JM (2004). Voltage-gated Na^+ channels confer invasive properties on human prostate cancer cells. *Pflugers Arch* **447**, 908–914.

Black JA, Cummins TR, Plumpton C, Chen YH, Hormuzdiar W, Clare JJ & Waxman SG (1999). Upregulation of a silent sodium channel after peripheral, but not central, nerve injury in DRG neurons. *J Neurophysiol* **82**, 2776–2785.

Blandino JK, Viglione MP, Bradley WA, Oie HK & Kim YI (1995). Voltage-dependent sodium channels in human small-cell lung cancer cells: role in action potentials and inhibition by Lambert–Eaton syndrome IgG. *J Membr Biol* **143**, 153–163.

Brackenbury WJ & Djamgoz MB (2003). Long-term exposure to tetrodotoxin suppresses voltage-gated Na^+ activity in the strongly metastatic MAT-LyLu rat prostate cancer cell line. *J Physiol* **552.P**, 102*P*.

Brackenbury WJ & Djamgoz MB (2004). Protein kinase A regulates functional expression of voltage-gated Na^+ channels in the strongly metastatic MAT-LyLu rat prostate cancer cell line. *J Physiol* **565.P**, PC115.

Brackenbury WJ & Djamgoz MB (2005). Activity-dependent regulation of voltage-gated Na^+ channels in the strongly metastatic MAT-LyLu rat prostate cancer cell line. *Biophys J* (Annual Meeting Abstracts), 459-Pos/B298.

Buchanan R, Nielsen OB & Clausen T (2002). Excitation- and β_2-agonist-induced activation of the Na^+–K^+ pump in rat soleus muscle. *J Physiol* **545**, 229–240.

Cantrell AR, Smith RD, Goldin AL, Scheuer T & Catterall WA (1997). Dopaminergic modulation of sodium current in hippocampal neurons via cAMP-dependent phosphorylation of specific sites in the sodium channel α subunit. *J Neurosci* **17**, 7330–7338.

Chang YC, Li PC, Chen BC, Chang MS, Wang JL, Chiu WT & Lin CH (2006). Lipoteichoic acid-induced nitric oxide synthase expression in RAW 264.7 macrophages is mediated by cyclooxygenase-2, prostaglandin E_2, protein kinase A, p38 MAPK, and nuclear factor-κB pathways. *Cell Signal* (in press DOI: 10.1016/j.cellsig.2005.1010.1005).

Cooper DM, Schell MJ, Thorn P & Irvine RF (1998). Regulation of adenylyl cyclase by membrane potential. *J Biol Chem* **273**, 27703–27707.

Dargent B & Couraud F (1990). Down-regulation of voltage-dependent sodium channels initiated by sodium influx in developing neurons. *Proc Natl Acad Sci U S A* **87**, 5907–5911.

Dargent B, Paillart C, Carlier E, Alcaraz G, Martin-Eauclaire MF & Couraud F (1994). Sodium channel internalization in developing neurons. *Neuron* **13**, 683–690.

Dib-Hajj S, Black JA, Felts P & Waxman SG (1996). Down-regulation of transcripts for Na channel α-SNS in spinal sensory neurons following axotomy. *Proc Natl Acad Sci U S A* **93**, 14950–14954.

Ding Y & Djamgoz MB (2004). Serum concentration modifies amplitude and kinetics of voltage-gated Na^+ current in the Mat-LyLu cell line of rat prostate cancer. *Int J Biochem Cell Biol* **36**, 1249–1260.

Diss JK, Archer SN, Hirano J, Fraser SP & Djamgoz MB (2001). Expression profiles of voltage-gated Na^+ channel α-subunit genes in rat and human prostate cancer cell lines. *Prostate* **48**, 165–178.

Diss JK, Stewart D, Pani F, Foster CS, Walker MM, Patel A & Djamgoz MB (2005). A potential novel marker for human prostate cancer: voltage-gated sodium channel expression in vivo. *Prostate Cancer Prostatic Dis* **8**, 266–273.

Djamgoz MBA, Mycielska M, Madeja Z, Fraser SP & Korohoda W (2001). Directional movement of rat prostate cancer cells in direct-current electric field: involvement of voltage gated Na^+ channel activity. *J Cell Sci* **114**, 2697–2705.

Fidler IJ (2003). Timeline: The pathogenesis of cancer metastasis: the 'seed and soil' hypothesis revisited. *Nat Rev Cancer* **3**, 453–458.

Fraser SP, Ding Y, Liu A, Foster CS & Djamgoz MB (1999). Tetrodotoxin suppresses morphological enhancement of the metastatic MAT-LyLu rat prostate cancer cell line. *Cell Tissue Res* **295**, 505–512.

Fraser SP, Diss JK, Chioni AM, Mycielska M, Pan H, Yamaci RF, Pani F, Siwy Z, Krasowska M, Grzywna Z, Brackenbury WJ, Theodorou D, Koyuturk M, Kaya H, Battaloglu E, Tamburo De Bella M, Slade MJ, Tolhurst R, Palmieri C, Jiang J, Latchman DS, Coombes RC & Djamgoz MB (2005). Voltage-gated sodium channel expression and potentiation of human breast cancer metastasis. *Clin Cancer Res* **11**, 5381–5389.

Fraser SP, Diss JK, Lloyd LJ, Pani F, Chioni AM, George AJ & Djamgoz MB (2004). T-lymphocyte invasiveness: control by voltage-gated Na^+ channel activity. *FEBS Lett* **569**, 191–194.

Fraser SP, Salvador V, Manning EA, Mizal J, Altun S, Raza M, Berridge RJ & Djamgoz MB (2003). Contribution of functional voltage-gated Na^+ channel expression to cell behaviors involved in the metastatic cascade in rat prostate cancer: I. Lateral motility. *J Cell Physiol* **195**, 479–487.

Grimes JA & Djamgoz MB (1998). Electrophysiological characterization of voltage-gated Na^+ current expressed in the highly metastatic Mat-LyLu cell line of rat prostate cancer. *J Cell Physiol* **175**, 50–58.

Grimes JA, Fraser SP, Stephens GJ, Downing JE, Laniado ME, Foster CS, Abel PD & Djamgoz MB (1995). Differential expression of voltage-activated Na^+ currents in two prostatic tumour cell lines: contribution to invasiveness in vitro. *FEBS Lett* **369**, 290–294.

Gu X, Lundqvist EN, Coates PJ, Thurfjell N, Wettersand E & Nylander K (2006). Dysregulation of TAp63 mRNA and protein levels in psoriasis. *J Invest Dermatol* **126**, 137–141.

Harootunian AT, Kao JP, Eckert BK & Tsien RY (1989). Fluorescence ratio imaging of cytosolic free Na^+ in individual fibroblasts and lymphocytes. *J Biol Chem* **264**, 19458–19467.

Herzog RI, Liu C, Waxman SG & Cummins TR (2003). Calmodulin binds to the C terminus of sodium channels Nav1.4 and Nav1.6 and differentially modulates their functional properties. *J Neurosci* **23**, 8261–8270.

Hilborn MD, Vaillancourt RR & Rane SG (1998). Growth factor receptor tyrosine kinases acutely regulate neuronal sodium channels through the src signaling pathway. *J Neurosci* **18**, 590–600.

Jin X & Gereau R IV (2006). Acute p38-mediated modulation of tetrodotoxin-resistant sodium channels in mouse sensory neurons by tumor necrosis factor-α. *J Neurosci* **26**, 246–255.

Kim J, Ghosh S, Liu H, Tateyama M, Kass RS & Pitt GS (2004). Calmodulin mediates Ca^{2+} sensitivity of sodium channels. *J Biol Chem* **279**, 45004–45012.

Klein JP, Tendi EA, Dib-Hajj SD, Fields RD & Waxman SG (2003). Patterned electrical activity modulates sodium channel expression in sensory neurons. *J Neurosci Res* **74**, 192–198.

Krasowska M, Grzywna ZJ, Mycielska ME & Djamgoz MB (2004). Patterning of endocytic vesicles and its control by voltage-gated Na^+ channel activity in rat prostate cancer cells: fractal analyses. *Eur Biophys J* **33**, 535–542.

Laniado ME, Lalani EN, Fraser SP, Grimes JA, Bhangal G, Djamgoz MB & Abel PD (1997). Expression and functional analysis of voltage-activated Na^+ channels in human prostate cancer cell lines and their contribution to invasion in vitro. *Am J Pathol* **150**, 1213–1221.

Lara A, Dargent B, Julien F, Alcaraz G, Tricaud N, Couraud F & Jover E (1996). Channel activators reduce the expression of sodium channel alpha-subunit mRNA in developing neurons. *Brain Res Mol Brain Res* **37**, 116–124.

Li M, West JW, Lai Y, Scheuer T & Catterall WA (1992). Functional modulation of brain sodium channels by cAMP-dependent phosphorylation. *Neuron* **8**, 1151–1159.

Livak KJ & Schmittgen TD (2001). Analysis of relative gene expression data using real-time quantitative PCR and the $2^{-\Delta\Delta CT}$ method. *Methods* **25**, 402–408.

Moody WJ & Bosma MM (2005). Ion channel development, spontaneous activity, and activity-dependent development in nerve and muscle cells. *Physiol Rev* **85**, 883–941.

Muniz M, Alonso M, Hidalgo J & Velasco A (1996). A regulatory role for cAMP-dependent protein kinase in protein traffic along the exocytic route. *J Biol Chem* **271**, 30935–30941.

Muniz M, Martin ME, Hidalgo J & Velasco A (1997). Protein kinase A activity is required for the budding of constitutive transport vesicles from the trans-Golgi network. *Proc Natl Acad Sci U S A* **94**, 14461–14466.

Murakami Y, Tanaka J, Koshimura K & Kato Y (1998). Involvement of tetrodoxin-sensitive sodium channels in rat growth hormone secretion induced by pituitary adenylate cyclase-activating polypeptide (PACAP). *Regul Pept* **73**, 119–121.

Mycielska ME, Fraser SP, Szatkowski M & Djamgoz MB (2003). Contribution of functional voltage-gated Na^+ channel expression to cell behaviors involved in the metastatic cascade in rat prostate cancer. II. Secretory membrane activity. *J Cell Physiol* **195**, 461–469.

Mycielska ME, Palmer CP, Brackenbury WJ & Djamgoz MB (2005). Expression of Na^+-dependent citrate transport in a strongly metastatic human prostate cancer PC-3M cell line: regulation by voltage-gated Na^+ channel activity. *J Physiol* **563**, 393–408.

Offord J & Catterall WA (1989). Electrical activity, cAMP, and cytosolic calcium regulate mRNA encoding sodium channel α subunits in rat muscle cells. *Neuron* **2**, 1447–1452.

Okuse K, Malik-Hall M, Baker MD, Poon WY, Kong H, Chao MV & Wood JN (2002). Annexin II light chain regulates sensory neuron-specific sodium channel expression. *Nature* **417**, 653–656.

Onganer PU & Djamgoz MB (2005). Small-cell lung cancer (human): potentiation of endocytic membrane activity by voltage-gated Na^+ channel expression in vitro. *J Membr Biol* **204**, 67–75.

Orphanides G & Reinberg D (2002). A unified theory of gene expression. *Cell* **108**, 439–451.

Paillart C, Boudier JL, Boudier JA, Rochat H, Couraud F & Dargent B (1996). Activity-induced internalization and rapid degradation of sodium channels in cultured fetal neurons. *J Cell Biol* **134**, 499–509.

Schedel J, Distler O, Woenckhaus M, Gay RE, Simmen B, Michel BA, Muller-Ladner U & Gay S (2004). Discrepancy between mRNA and protein expression of tumour suppressor maspin in synovial tissue may contribute to synovial hyperplasia in rheumatoid arthritis. *Ann Rheum Dis* **63**, 1205–1211.

Shah BS, Rush AM, Liu S, Tyrrell L, Black JA, Dib-Hajj SD & Waxman SG (2004). Contactin associates with sodium channel Nav1.3 in native tissues and increases channel density at the cell surface. *J Neurosci* **24**, 7387–7399.

Sherman SJ & Catterall WA (1984). Electrical activity and cytosolic calcium regulate levels of tetrodotoxin-sensitive sodium channels in cultured rat muscle cells. *Proc Natl Acad Sci U S A* **81**, 262–266.

Sherman SJ, Chrivia J & Catterall WA (1985). Cyclic adenosine 3′:5′-monophosphate and cytosolic calcium exert opposing effects on biosynthesis of tetrodotoxin-sensitive sodium channels in rat muscle cells. *J Neurosci* **5**, 1570–1576.

Shiraishi S, Yokoo H, Yanagita T, Kobayashi H, Minami S, Saitoh T, Takasaki M & Wada A (2003). Differential effects of bupivacaine enantiomers, ropivacaine and lidocaine on up-regulation of cell surface voltage-dependent sodium channels in adrenal chromaffin cells. *Brain Res* **966**, 175–184.

Smith R & Goldin AL (1997). Phosphorylation at a single site in the rat brain sodium channel is necessary and sufficient for current reduction by protein kinase A. *J Neurosci* **17**, 6086–6093.

Smith KE, Gibson ES & Dell'Acqua ML (2006). cAMP-dependent protein kinase postsynaptic localization regulated by NMDA receptor activation through translocation of an A-kinase anchoring protein scaffold protein. *J Neurosci* **26**, 2391–2402.

Smith P, Rhodes NP, Shortland AP, Fraser SP, Djamgoz MB, Ke Y & Foster CS (1998). Sodium channel protein expression enhances the invasiveness of rat and human prostate cancer cells. *FEBS Lett* **423**, 19–24.

Sola B, Salaun V, Ballet JJ & Troussard X (1999). Transcriptional and post-transcriptional mechanisms induce cyclin-D1 over-expression in B-chronic lymphoproliferative disorders. *Int J Cancer* **83**, 230–234.

St Johnston D (2005). Moving messages: the intracellular localization of mRNAs. *Nat Rev Mol Cell Biol* **6**, 363–375.

Tiedge H, Bloom FE & Richter D (1999). RNA, whither goest thou? *Science* **283**, 186–187.

Ungefroren H, Cikos T, Krull NB & Kalthoff H (1997). Biglycan gene promoter activity in osteosarcoma cells is regulated by cyclic AMP. *Biochem Biophys Res Commun* **235**, 413–417.

Vijayaragavan K, Boutjdir M & Chahine M (2004). Modulation of Nav1.7 and Nav1.8 peripheral nerve sodium channels by protein kinase A and protein kinase C. *J Neurophysiol* **91**, 1556–1569.

Wada A, Yanagita T, Yokoo H & Kobayashi H (2004). Regulation of cell surface expression of voltage-dependent Nav1.7 sodium channels: mRNA stability and posttranscriptional control in adrenal chromaffin cells. *Front Biosci* **9**, 1954–1966.

Waechter CJ, Schmidt JW & Catterall WA (1983). Glycosylation is required for maintenance of functional sodium channels in neuroblastoma cells. *J Biol Chem* **258**, 5117–5123.

Wakabayashi I, Marumo M & Sotoda Y (2003). Diverse effects of monensin on capacitative Ca^{2+} entry and release of stored Ca^{2+} in vascular smooth muscle cells. *Eur J Pharmacol* **464**, 27–31.

Waxman SG (2001). Transcriptional channelopathies: an emerging class of disorders. *Nat Rev Neurosci* **2**, 652–659.

Waxman SG, Kocsis JD & Black JA (1994). Type III sodium channel mRNA is expressed in embryonic but not adult spinal sensory neurons, and is reexpressed following axotomy. *J Neurophysiol* **72**, 466–470.

Yang BC, Lin HK, Hor WS, Hwang JY, Lin YP, Liu MY & Wang YJ (2003). Mediation of enhanced transcription of the IL-10 gene in T cells, upon contact with human glioma cells, by Fas signaling through a protein kinase A-independent pathway. *J Immunol* **171**, 3947–3954.

Yoshida K, Kanaoka S, Takai T, Uezato T, Miura N, Kajimura M & Hishida A (2005). EGF rapidly translocates tight junction proteins from the cytoplasm to the cell-cell contact via protein kinase C activation in TMK-1 gastric cancer cells. *Exp Cell Res* **309**, 397–409.

Yuhi T, Wada A, Kobayashi H, Yamamoto R, Yanagita T & Niina H (1996). Up-regulation of functional voltage-dependent sodium channels by cyclic AMP-dependent protein kinase in adrenal medulla. *Brain Res* **709**, 37–43.

Zhang X, Odom DT, Koo SH, Conkright MD, Canettieri G, Best J, Chen H, Jenner R, Herbolsheimer E, Jacobsen E, Kadam S, Ecker JR, Emerson B, Hogenesch JB, Unterman T, Young RA & Montminy M (2005). Genome-wide analysis of cAMP-response element binding protein occupancy, phosphorylation, and target gene activation in human tissues. *Proc Natl Acad Sci U S A* **102**, 4459–4464.

Zhou J, Yi J, Hu N, George AL Jr & Murray KT (2000). Activation of protein kinase A modulates trafficking of the human cardiac sodium channel in *Xenopus* oocytes. *Circ Res* **87**, 33–38.

Acknowledgements

This work was funded by a MRC Priority Area (Prostate Cancer) PhD studentship and the Pro Cancer Research Fund (PCRF). We thank Dr Kenji Okuse for giving useful advice on the manuscript.